Sensing Fruit Ripeness Using Wireless Signals

Sheng Tan, Linghan Zhang, Jie Yang
Florida State University, Tallahassee, Florida, USA
{tan, lzhang, jie.yang}@cs.fsu.edu

***Abstract*—This paper presents FruitSense, a novel fruit ripeness sensing system that leverages wireless signals to enable non-destructive and low-cost detection of fruit ripeness. Such a system can reuse existing WiFi devices in homes without the need for additional sensors. It uses WiFi signals to sense the physiological changes associated with fruit ripening for detecting the ripeness of fruit. FruitSense leverages the larger bandwidth at 5GHz (i.e., over 600MHz) to extract the multipath-independent signal components to characterize the physiological compounds of the fruit. It then measures the similarity between the extracted features and the ones in ripeness profiles for identifying the ripeness level. We evaluate FruitSense in different multipath environments with two types of fruits (i.e, kiwi and avocado) under four levels of ripeness. Experimental results show that FruitSense can detect the ripeness levels of fruits with an accuracy over 90%.**

I. Introduction

Recent advances in wireless technology have greatly expanded the WiFi usage from providing laptop connectivity to connecting mobile and smart devices to the Internet and home networks. Such an evolution has resulted in the prevalence of WiFi devices, which provides opportunities to extend WiFi's capabilities beyond communication, particularly in human sensing. As the wireless signals travel through space, they interact with human body and undergo wave phenomena such as reflection and diffraction. These phenomena lead to multipath effects, which carry a rich set of information about the physical environment including the human location and activities. Indeed, there has been a growing interest in using multipath effects to perform human sensing, ranging from large scale movements [30], [25], to small scale motions [5], [27], [19], and location [28], [4], [29].

In this work, we further expand the WiFi sensing capabilities from human sensing to sensing bio-information of fruits. In particular, we seek to sense the degree of ripeness in fruits with WiFi signals. Monitoring the ripeness of fruit provides many benefits for several end-users, ranging from farmers, to distributors, retailers and consumers. It can help farmers to determine the optimal harvest time as the quality heavily depends on when they are harvested. It can also assist fruit distributors in performing rapid sorting in storage facilities and deciding when to send their stock during post-harvest period. Retailers can minimize losses and maintain fruit quality through effective selling strategies based on accurate categorization of the fruit ripeness. Monitoring the ripeness of fruits throughout the supply chain thus can reduce waste as well as improve the consistency of quality for consumers.

In this paper, we focus on inferring the ripeness of fruit for consumers. As indicated in previous study from 2011 [10], in north America, compare to a 12% loss of fruits and vegetables in distribution and retail process, the loss rate is 28% after customer purchase. This is due to fruits are sensitive to various environmental factors such as temperature, air ventilation, and illumination condition. Those factors are very difficult to control especially within normal household environments. Moreover, ordinary consumers lack the professional knowledge and equipment for accurately judging fruit ripeness level by appearance. Monitoring the ripeness level of fruits thus can benefit customers by avoiding the unpleasantness of tart or rotten fruit and eventually reduce the waste.

The challenge in monitoring the ripeness of fruit for consumers lies in finding solutions that can provide non-destructive testing at minimal cost. Existing approaches for inferring the ripeness of fruit mainly depend on penetrometer [11], refractometer [12], or spectrometer [20]. While the penetrometer measures fruit firmness by quantifying the force required to insert a probe into the fruit [11], refractometer (e.g., Brix [12]) analyzes sugar content of the juice using light refraction. Both methods, however, are destructive and less acceptable to consumers. In contrast, spectrometer based approach is non-destructive. It splits light signals into a fruit and then measures the light that is emitted, absorbed or scattered by the fruit for ripeness inference [20]. However, traditional spectrometer instruments are bulky and expensive (i.e., costing several thousands of dollars) and are limited to controlled laboratory settings [20].

More recent work includes using advanced imaging techniques and ultrasonic measurement systems to analyze the image features (e.g., color and texture) and measure the ultrasonic attenuation of the fruit for ripeness detection [14], [3], respectively. However, these methods require specialized equipments, and are less accessible to ordinary consumers. Recently, due to advances in materials and fabrication techniques, portable spectrometers that work together with smartphones have been realized. For example, Das *et al.* [8] propose a smartphone based spectrometer that can measure UV fluorescence of Chlorophyll found in apples, whereas the company Consumer Physics develops the sensor SCiO that can be integrated with smartphones to analyze the molecular composition of food [2], [1]. Although these portable solutions can be adapted by consumers, there also are non-negligible costs incurred in purchasing dedicated spectral sensors.

In this paper, we introduce FruitSense, a novel method for inferring the ripeness of fruit for consumers that is both non-destructive and low-cost. FruitSense uses WiFi signals to sense the physiological changes associated with fruit ripening

978-1-5386-5156-8/18/$31.00 ©2018 IEEE

for ripeness detection. It allows users to reuse off-the-shelf WiFi devices for ripeness monitoring, and thus can enable large-scale deployment and benefit a large number of users by leveraging the proliferation of WiFi devices and networks.

In particular, fruit ripening involves a series of physiological changes leading to the development of a soft edible ripe fruit. Take avocado as an example, there are changes in the total dry matter and moisture content during maturation and ripening. As moisture content decreases, the dry matter increases accordingly. When wireless signals travel through a fruit, the changes in the physiological compounds of the fruit during ripening lead to distinct and measurable effects on the received signals. We thus can infer the ripeness level based on the physiological changes interpreted by the received signals.

Accurately discerning the ripeness of fruit is challenging, however, when using a single pair of off-the-shelf WiFi devices. First, the measurable changes in the received signals due to fruit ripening are subtle, and the impact of fruit size on the received signals might distort such changes. To address these issues, we leverage frequency diversity by probing the fruit with WiFi signals at multiple frequency channels. Leveraging frequency diversity not only provides a rich set of information to capture the subtle changes, but also enables us to examine the change pattern among multiple channels, instead of a single channel, to mitigate the impact of fruit size.

Addtionaly, signal propagation is dominated by multipath in typical indoor environments when the line-of-sight (LOS) is blocked by fruit during the ripeness sensing process. While the WiFi based human sensing primarily relies on the signal reflections, the reflected signals from surroundings represent interferences to the signal component indicating the ripeness of fruit. Once the indoor environment changes, the changes in the received signals mainly reflect the differences in multipath propagation instead of the physiological change of the fruit. To accurately capture the changes corresponding to fruit ripening, we propose to extract the multipath-independent signal components for ripeness sensing by isolating the signal component traveling through the fruit directly, from the ones reflected from the surrounding environment. Specifically, we leverage the larger bandwidth at 5GHz (i.e., over 600MHz) to derive fine-grained power delay profile for extracting the signals that directly went through the fruit from the multipath propagation.

Moreover, as the usable WiFi channels in 5GHz are unequally and non-contiguous spaced, the inverse non-uniform Discrete Fourier Transform (NDFT) is used to derive the fine-grained power delay profile. However, there are various uncertainties introduced from the inverse NDFT as it relies on proximal gradient methods to find solutions to an under determined system. To mitigate such uncertainties, we propose to use the Maximal Overlap Discrete Wavelet Transform (MODWT) for multi-resolution feature analysis, which is not sensitive to the uncertainties such as the starting and ending points (and possibly outliers) of a series of signal.

More specifically, our system first probes the fruit with WiFi signals hopping at all available 5GHz channels. The sampled channel frequency response, which is exported by the WiFi NICs in the form of Channel State Information (CSI), then goes through the calibration process to correct errors due to hardware limitation of WiFi NICs. We then stitch together the calibrated CSI from each individual channel. Due to the usable WiFi channels in 5GHz are unequally and non-contiguous spaced, the inverse NDFT is used to derive the fine-grained power delay profile for multipath removal. Next, we identify and extract the signals that directly went through the fruit for ripeness detection. At last, we use the Maximal Overlap Discrete Wavelet Transform (MODWT) to extract signal features over multiple channels at multiple resolutions and compare the features against known ripeness profiles that identify the degree of ripeness.

We evaluate FruitSense in different multipath environments with two types of fruit: *kiwi* and *avocado*. The fruit samples are purchased from two venders with different ripeness levels. The volume of each type of fruit is about 75 at each ripeness level. We identify the ripeness as one of the four levels: *unripen*, *half ripen*, *ripen* and *over ripen*. Experimental results show that FruitSense is highly effective in detecting fruit ripeness. It achieves an accuracy at over 90% in identifying the ripeness level of fruit.

The main contributions are summarized as follows.

- We show that the WiFi signals can be utilized to capture the physiological changes of fruit for ripeness detection. The system is non-destructive and low-cost, without the need for additional sensors.
- We leverage frequency diversity to capture the physiological changes of the fruit, and utilize the larger bandwidth at 5GHz to combat multipath for extracting multipath-independent signal components for ripeness detection. We further utilize MODWT to extract features over multiple frequencies for identifying the level of fruit ripeness.
- We conduct extensive experiments in different multipath environments with two typical fruits under various conditions. Experimental results show that FruitSense achieves around 90% ripeness level detection accuracy.

II. Preliminaries

A. Fruit Ripening

There exists two types of fruits according to the regulatory mechanisms underlying their ripening process: climacteric and non-climacteric fruits. Climacteric fruits, such as kiwi, avocado, apple and banana will continue to ripen after the fruit has left the plant; however, non-climacteric fruits, such as grape, orange and pineapple stop the ripening process the minute they leave the plant [24]. In this work, we focus on sensing the ripeness of climacteric fruits, as we do not have the access to the non-climacteric fruits that are on the plants. Nevertheless, our system can be extended to sensing the maturity of non-climacteric fruits during the growth and development process while they are on the plants.

Fruit ripening is a highly coordinated and an irreversible phenomenon involving a series of physiological and organoleptic changes [24]. For example, some fruits, such as

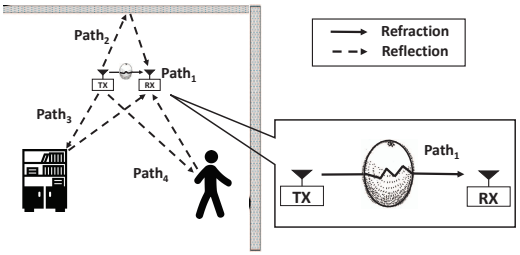

Fig. 1. Multipath propagations in an indoor environment during fruit ripeness sensing.

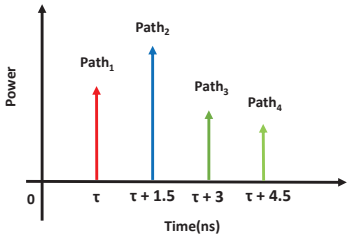

Fig. 2. Combining all the channels at 5GHz provides a power delay profile with sufficient resolution to differentiate multipath propagations.

banana and apple, come in a wide array of colors that change throughout their ripening process, with the brightest colors often occurring when the fruit is optimally ripened. Such color changes enable people to predict the ripeness level based on external visual inspection. By contrast, some other fruits, like kiwi and avocado, do not exhibit obvious organoleptic changes during the ripening process. It is hard for ordinary people to tell the ripeness level based on organoleptic testing. We thus focus on kiwi and avocado and seek to sense the ripeness based on physiological changes, instead of organoleptic changes.

Existing work uses the physiological changes such as oil context, dry matter and moisture content to determine the ripeness of avocado [20]. Specifically, oil content and dry matter increase during development and continue to change during ripening [20]. As oil content increases, the moisture content decreases by the same amount, so that the total percentage of oil and moisture content remains constant. Similarly, the content change within dry matter can be used to track the ripeness of kiwi fruit [24]. In particular, dry matter of kiwi is mainly comprised by the carbohydrates and starch, which gradually transform to soluble solids such as sugar content during the ripening. The percentage of carbohydrates and starch thus could be used as an indicator of fruit ripeness.

B. WiFi Sensing based Approach

Figure 1 illustrates a typical experimental setup of sensing fruit ripeness using a pair of WiFi devices in an indoor environment. The testing fruit is placed in between a pair of closely spaced transmitter and receiver, thus blocking the line-of-sight (LOS) signal propagation. We rely on the received signal component that directly travels through the fruit to sense its physiological change. The phenomenon where radio waves travel through and modulated by the fruit is commonly referred as refraction, which describes the signal passes from one medium to another. In our case, it is the WiFi signal travels from air to fruit, and then from fruit to air.

To quantify the effect of the refraction, we could leverage the concept of permittivity, which is a measure of how an electric field affects, and is affected by, a dielectric medium (i.e, the fruit in our case). In particular, the complex relative permittivity ε^* of a material to that of free space in frequency domain can be described as following [18]:

$$\varepsilon^* = \varepsilon^{'} - j\varepsilon^{''} \tag{1}$$

The real part $\varepsilon^{'}$ is referred to as the dielectric constant, which describes the ability of the material to store energy when it is exposed to an electric field. The imaginary part $\varepsilon^{''}$ is referred to as dielectric loss factor, and $j = \sqrt{-1}$. The dielectric loss factor influences both energy attenuation and absorption, and is commonly used to describe the ability of the material to dissipate electrical energy as heat.

As fruit ripening involves a series of physiological changes, fruit at different ripeness levels results in different dielectric constants and loss factors. The permittivity of the fruit thus could be used as an indicator of its internal quality. Indeed, there exists prior work on using expensive and dedicated dielectric spectroscopy to measure the dielectric properties of fruit and vegetable for internal quality analysis [17].

As we use the off-the-shelf WiFi devices, we exam how the received signal changes due to the changed physiological compounds of the fruit. Specifically, when the WiFi signal travels through the fruit, the electric field strength decreases with the distance from its surface. To quantify such an effect, the attenuation factor α, which depends on the dielectric properties of the fruit, could be leveraged. It is given by:

$$\alpha = \frac{2\pi}{\lambda_0}\left[\frac{1}{2}\varepsilon^{'}\left(\sqrt{1+\left(\frac{\varepsilon^{''}}{\varepsilon^{'}}\right)^2}-1\right)\right]^{1/2} \tag{2}$$

where λ_0 is the free-space wavelength of the WiFi signal [18]. Based on Equation 2, we know that the fruits at different ripeness levels lead to different attenuation factors, which could be measured by analyzing the received signals. Therefore, instead of using dedicated dielectric spectroscopy, we leverage the received signal that directly travels through the fruit for ripeness detection.

Excepting for the controllable experimental settings such as the location of the fruit in between the transmitter and the receiver, the sizes of the fruit could be slightly different, which may affect the signal attenuation as well. Note that from Equation 2, we can observe that the WiFi signals at different frequencies (wavelengths) result in different attenuation factors as well. We thus can leverage the frequency diversity by probing the fruit at multiple channels, and then analyze the relative changes between multiple frequencies to mitigate the impact of fruit size.

C. Practical Issues

While the intuition is simple, there are significant challenges to accurately capture the received signal that directly travels through the fruit for extracting the multipath-independent features that characterize the physiological compounds of the fruit. As shown in Figure 1, besides the signal refraction, there

exists signal reflections. The signals that reflected from the walls, furniture, and human body will be combined with the signal travels through the fruit at the receiver. This leads to the fact that the measured signals at the receiver mainly reflect the multipath environments. Thus it is highly sensitive to environment changes. To make the system robust to the multipath propagation, we need to separate the signal component that travels through the fruit from the reflected ones.

Intuitively, this can be done by leveraging the power delay profile, which gives the power intensity of received signals as a function of propagation delay. By performing Inverse Fast Fourier Transform (IFFT) of the received signal measurements, we are able to extract the first arriving signal, which travels through the shortest path among all the paths from the transmitter to the receiver. However, the widely used bandwidth of a WiFi channel is either 20MHz or 40MHz, which results in a power delay profile with a resolution at either 50ns or 25ns. Given that the wireless signal travels at the speed of light, such resolutions correspond to distance resolutions of 15m and 7.5m, respectively. In typical indoor environments, a majority of the reflected signals have path lengths smaller than 15m or 7.5m. Therefore, the obtained first arriving signal based on each channel is still a mixture of the signals that travel through the fruit and multipath. Therefore, simply performing IFFT on the signal measurements at each WiFi channel provides insufficient time or distance resolution for extracting the signal traveling through the fruit.

As WiFi spans multiple channels at both 2.4GHz and 5GHz, we propose to probe the fruit at all available channels of 5GHz with larger bandwidth. Combining all the channels at 5GHz (i.e., from 5.18GHz to 5.825GHz) brings over 600MHz bandwidth, which corresponds to a 1.5ns time resolution or to a 0.45 meters distance resolution. Such a high resolution is sufficient for us to separate the signal traveling through the fruit from the reflected ones, as shown in Figure 2. Given the signal measurements at each channel, we then stitch these measurements together to derive a fine-grained power delay profile for multipath removal.

One problem with that stitching lies in the fact that the usable WiFi channels at 5GHz are unequally and non-contiguous spaced due to FCC regulation. For example, the channels from 120 to 128 are partially occupied by the weather radar usage in the US, and different countries apply their own regulations. Venders usually disable some of the 5GHz channels in compliance with the regulations of different countries before shipping the WiFi NICs. We thus cannot simply use IFFT, which only works for uniformly-spaced frequency measurements. To overcome this issue, we adopt the inverse non-uniform Discrete Fourier Transform (NDFT), which is capable of deriving a fine-grained power delay profile from non-uniformly spaced channels at 5GHz.

Another challenge lies in the feature extraction process for ripeness level identification. This is because various uncertainties are introduced by the process of solving an under determined system with inverse NDFT across different samples. Such uncertainties could result in inconsistent features from various samples. To overcome such challenge, we utilize Maximal Overlap Discrete Wavelet Transform (MODWT), which is shift invariant and is not sensitive to the starting and ending points (and possibly outliers) of the data. By utilizing MODWT, we are able to minimize the uncertainty caused by NDFT and extract consistent features from given samples.

III. System Design

A. System Overview

Our system uses a pair of WiFi devices to sense the physiological compounds of fruit for ripeness detection. Figure 3 illustrates the flow of our system. It first probs the fruit with WiFi signals hopping through all usable channels at 5GHz. The system then collects the sampled channel frequency response in the form of Channel State Information (CSI) including the information of phase and amplitude. The CSI measurements are reported by the WiFi NIC at the receiver.

The CSI measurements are then preprocessed to calibrate both the phase and amplitude errors. In particular, the raw phase contains residual synchronization errors, which are composed of two types of errors: linear errors with respect to the subcarrier indexes and the constant errors across subcarriers. Our system calibrates the linear phase errors by searching for an optimum phase compensation value that minimizes the differences in the derived power delay profiles across multiple channels. The constant phase errors and amplitude errors could be mitigated by averaging the measurements of multiple packets that received in the coherence time window.

Given the calibrated CSI measurements, our system performs multipath removal for extracting the signal that directly travels through the fruit. Our system stitches the CSI measurements of all the channels together to enlarge the bandwidth for improving the resolution of the power delay profile. The inverse NDFT technique is used to overcome the problem of the unequal and non-contiguity spacing of 5GHz channels. Our system then identifies and extracts the signal directly travelling through the fruit for ripeness detection.

At last, our system identifies the fruit ripeness level by measuring the similarity between the extracted features and the pre-built ripeness profiles. The MODWT is used to extract features over multiple channels and the cross correlation is used to compare the features against the ripeness profiles in the library. The testing fruit is identified as one of the following ripeness levels: *unripen*, *half ripen*, *ripen* and *over ripen*.

B. CFR Sampling and Data Calibration

With 802.11n/ac systems, the WiFi NICs track fine-grained channel state information, which is a sampled version of the channel response including both phase and amplitude information. On the standard 20MHz WiFi channel, it measures the amplitude and phase for each of the 56 OFDM subcarriers. With wider 40MHz channels, CSI measurements are available for 128 subcarriers. In our work, we utilize all available 20MHz WiFi channels at 5GHz. To ensure that the channel hopping goes through all the channels within the coherence time, the hopping delay is set as 0.25ms. Note that

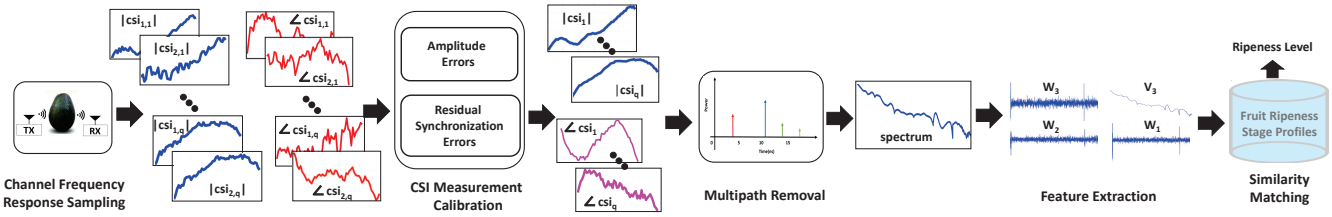

Fig. 3. System Overview.

the coherence time in typical indoor environment is around 300ms [9]. This allows us to collect multiple packets at each channel within the coherence time.

In particular, we denote $\mathbf{csi_{p,q}}$ as the CSI complex vector sampled at the p^{th} packet of the q^{th} channel. Each CSI complex vector in frequency domain can be represented as:

$$\mathbf{csi}_{p,q} = [csi^1_{p,q}, csi^2_{p,q}, \cdots, csi^K_{p,q}], \tag{3}$$

where K is the total number of subcarriers reported at each channel per packet (i.e., K = 56) and $csi^k_{p,q}$ is the sampled channel response at the k^{th} subcarrier.

Since the CSI measurements are extracted by sampling the channel frequency response, the raw CSI measurements incur significant distortions due to the hardware limitations of off-the-shelf WiFi NICs. Thus the reported CSI phase measurement $\angle\mathbf{csi}^k_{p,q}$ can be further represented as:

$$\angle\mathbf{csi}^k_{p,q} = \angle\mathbf{h}^k_{p,q} + k\varphi_l + \varphi_c, \tag{4}$$

where $\angle\mathbf{h}^k_{p,q}$ represents the phase rotation due to signal propagation, φ_l denotes the slope of the linear phase error and φ_c is the constant phase shift error.

As our system relies on the CSI measurements to derive fine-grained power delay profile for multipath removal, we need to correct errors in the CSI measurements. First, the amplitude error is discovered to follow Gaussian distribution [15], it could be mitigated by averaging CSI measurements from multiple packets that within the coherence time [32]. The constant phase error φ_c, is caused by the residual central frequency offset. We select a reference channel from all the available channels and mitigate it through correcting the phase difference from each channel. The linear phase error φ_l is a frequency dependent error and can be further divided into two components: $\varphi_l = \varphi_d + \varphi_s$. The phase error φ_d is observed to follow the Gaussian distribution with zero mean [15]. Thus can be mitigated by averaging multiple CSI phase measurements collected at each channel [32].

The second component φ_s is introduced by the residual sampling frequency offset [15]. After removing phase errors φ_c and φ_d and assuming the phase compensation for φ_s is $\varphi_s^{'}$, Equation 4 can be rewritten as:

$$\angle\widehat{\mathbf{csi}^k_{p,q}} = \angle\mathbf{h}^k_{p,q} + k\varphi_s - k\varphi_s^{'}. \tag{5}$$

By gradually changing the value of $\varphi_s^{'}$, different power delay profiles can be derived for each channel. The optimum phase compensation φ_s can be found when the differences in derived power delay profiles across multiple channels are minimized. In particular, it can be formulated as an optimization problem as following:

$$\min_{\varphi_s^{'}} \sum_{q,q^{'}=1}^{Q} ||\mathbf{g}_q(\varphi_s^{'}) - \mathbf{g}_{q^{'}}(\varphi_s^{'})||^2, \ q \neq q^{'}, \tag{6}$$

where $\mathbf{g_q}(\varphi_s^{'})$ denotes the derived power delay profile at the qth channel and Q is the total number of channels. By obtaining an optimum value of $\varphi_s^{'}$, we are able to remove the linear phase error φ_s from the CSI phase measurements.

Figure 5(a) shows the phases across different channels after calibrating φ_s. As shown in Figure 5(a), after calibration, the phases of the overlapped subcarriers at three different 2.4GHz band channels now demonstrate similarity and consistency. Thus we can pick either channel as reference to stitch them together. Figure 5(b) shows three non-overlapping channels at 5GHz band after phase calibration.

C. Multipath Removal

Multipath removal leverages a fine-grained power delay profile to extract the signal that directly travels through the fruit for ripeness detection. Since a power delay profile derived from one single WiFi channel provides insufficient time delay resolution, our system stitches all the available channels at 5GHz together to improve the resolution for extracting the signal that travels through the shortest path.

Due to the regulations at many countries, the usable channels at 5GHz are unequally and non-contiguous spaced. For example, the usable channels at 5GHz on the Atheros NICs are separated into four segments. The venders disabled some channels in compliance with the local regulations. We thus cannot simply use IFFT for power delay profile derivation, as it only works for uniformly-spaced frequency measurements. Instead, we adopt inverse Non-uniform Discrete Fourier Transform (NDFT), which works for non-uniformly spaced channels [28]. For fine-grained power profile derivation, given the calibrated CSI measurements from last step as:

$$\mathbf{CSI} = [\widehat{\mathbf{CSI}}_1, ..., \widehat{\mathbf{CSI}}_q, ...], \tag{7}$$

where q denotes the qth channel, we can formulate the inverse NDFT as following:

$$\min_{\mathbf{g}} ||\mathbf{CSI} - \mathcal{F}\mathbf{g}||^2, \tag{8}$$

where $\mathbf{g}$ represents the power delay profile that we search for, $\mathcal{F}$ is Fourier matrix. The goal is to find an optimum solution of $\mathbf{g}$ that minimizes the difference between $\mathbf{CSI}$ and Fourier Transform of $\mathbf{g}$.

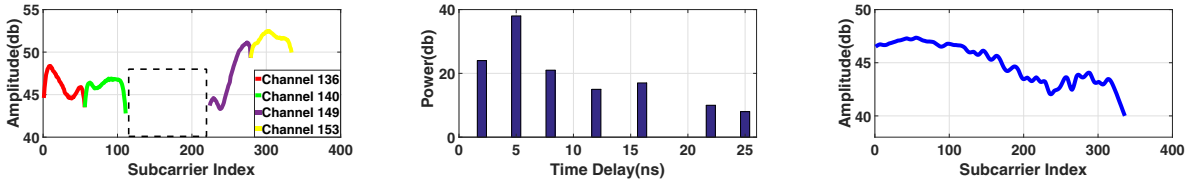

(a) Before multipath removal (b) Derived power delay profile (c) After multipath removal

Fig. 4. The CSI amplitude for four channels with gap at 5GHz before and after multipath removal.

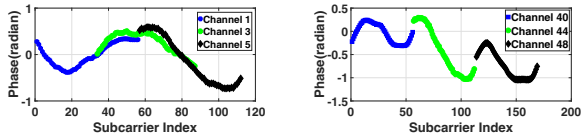

(a) 2.4GHz (b) 5GHz

Fig. 5. Calibrated CSI phases for three overlapping channels at 2.4GHz and three channels at 5GHz.

Such an optimization problem can be viewed as an under-determined system, which yields several possible solutions. To pick the best one, we need to add constraints to filter out the less desired ones. To find constraints, we look into the characteristic of signal propagation in indoor environment. Based on previous observations [28], although multiple paths exist in typical indoor environment, only a few paths would dominate the signal propagation. It is because they travel through shorter paths and suffer less attenuations when comparing to longer ones. We thus add one constraint to the inverse NDFT: among all the solutions of $\mathbf{g}$ that satisfy Equation 8, our system favors the $\mathbf{g}$ with fewer dominating propagation paths.

To solve the Equation 8 with the constraint, we adopt the proximal gradient method that used to solve convex optimization problem [13]. In particular, our system takes $\mathbf{CSI}$ as input and computes the gradient of differentiable term in Equation 8. After obtaining several solutions, our system selects the one that with fewer dominating paths. Given the derived fine-grained power delay profile, we remove the components from multipath propagations and only keep the component that goes through the fruit directly. Then, we covert the trimmed power delay profile back to frequency domain for feature extraction.

Figure 4 shows the amplitude of the channels cover the same bandwidth before and after multipath removal. As shown in Figure 4(a), four channels at 5GHz band cover 100MHz bandwidth with a 40MHz gap in between as highlighted by a black dot rectangle. After performing inverse NDFT, we are able to derive a fine-grained power delay profile shown in Figure 4(b), which indicated the lack of LoS. Then we remove the multipath components from the power delay profile, only reserve the signal propagation affect by fruit and convert it back to frequency domain. The resulting spectrum is shown in Figure 4(c). We observe that the amplitude continues to decrease with the increasing frequency. It is consistent with Equation 2, and shows that a higher frequency would suffer a larger attenuation when propagating through the fruit.

D. Feature Extraction and Ripeness Identification

After multipath removal process, we obtained the signal in frequency domain over 600MHz bandwidth that mainly affected by fruit. Next we need to extract features to identify the ripeness level by comparing them to the existing profile. Intuitively, this can be done by adopting varies techniques from existing works. However, the frequency domain signal from previous step were calculated using NDFT which introduces various uncertainty across different signal samples. This is caused by the nature of using proximal gradient method to solve under determined system problem. Since various uncertainty over 600MHz bandwidth signal across different samples would lead to inconsistent feature extraction. This might compromise the ripeness level identification process.

To overcome such problem, our system thus adopts Maximal Overlap Discrete Wavelet Transform (MODWT) [23] to extract features based on the signals that travel through fruit at multiple frequencies (i.e., spectrum). First, MODWT is shift invariant, which means the decomposition outputs stay invariant on different starting and ending points. This enables us to retrieve consistent features across a large number of samples with various uncertainty. Second, the redundancy of MODWT facilitates detail preservation of the original sample for multiple level decomposition process.

In particular, MODWT analyzes the signals in both time and frequency domains by decomposing signals into successive approximation coefficients along with detailed coefficients. The approximation coefficients depict the large scale characteristic of change pattern, whereas the detailed coefficients capture small scale components that represent the fine details of the changes. Given a signal $\mathbf{X(i)}$, each level of MODWT coefficients are computed based on the following equations:

$$\begin{aligned} W_{j,i} &= \sum l = 0^{L-1} h_{j,l} X_{i-l mod N}, \\ V_{j,i} &= \sum l = 0^{L-1} g_{j,l} X_{i-l mod N}, \end{aligned} \tag{9}$$

where $V_{j,i}$ is the approximation coefficient and $W_{j,i}$ is the detailed coefficient. Here $h_{j,l}$ and $g_{j,l}$ are the wavelet filter and scaling filter respectively. j is the level of decomposition and $l = 1...L$ is the length of the filter. By applying MODWT to the extracted signal at each channel recursively for 3 levels, we obtain both large scale and detailed features.

To identify the degree of ripeness, we utilize cross correlation to calculate the similarity between the extracted features and the ones in the profile library. It measures the similarity based on the relative changes and is independent of translations and scaling in the amplitude. This is done repeated over 3 levels of approximation and detailed features and combined using empirically assigned weights. The ripeness level with the profile in the library that has the highest similarity with the testing fruit is then identified as the detected ripeness level.

Fruit / Ripeness	Kiwi		Avocado	
	Vendor 1	Vendor 2	Vendor 1	Vendor 2
Unripen	48	32	45	35
Half Ripen	43	31	43	33
Ripen	44	32	40	34
Over Ripen	42	30	44	34

Fig. 6. Volumes of fruits in our evaluation.

IV. Performance Evaluation

In this section, we describe our experimental setup and evaluate the performance of FruitSense in detecting the ripeness level of Kiwi fruit and Avocado under different environments.

A. Experiment Setup

We conduct experiments with two laptops (i.e., Dell LATITUDE E5540), each connecting with an external antenna. The distance between two external antennas is about 20cm. The testing fruit is placed in the middle of the two antennas, thus blocking the line-of-sight propagation. Both laptops run Ubuntu 12.04 LTS and are equipped with the WiFi NICs of Atheros AR9580 for extracting CSI measurements [32]. The transmitter and receiver hop through all available 20MHz WiFi channels at 5GHz bands in an 802.11n network. There are total 21 available channels enabled by the Atheros AR9580 card. And they fall into four non-contiguous segments. The first segment is from 5.18GHz to 5.32 GHz (i.e., the channels from 36 to 64), whereas the second segment is from 5.5GHz to 5.58 GHz (i.e., the channels from 100 to 116). The third one and forth one are from 5.66GHz to 5.7 GHz (i.e., the channels from 132 to 140) and from 5.745GHz to 5.825GHz (i.e., the channels from 149 to 165), respectively.

Although the entire 5GHz has the bandwidth over 600MHz, we can only obtain 420MHz bandwidth from these four segments. We thus need to use inverse NDFT to derive the power delay profile for over 600MHz bandwidth based on unequally and non-contiguous spaced 21 channels. The channel hopping delay is set as 0.25ms. As the coherence time in typical indoor environment is about several hundreds milliseconds [9], we can collect packets across channels within coherence time as well as obtain multiple packets at each channel within coherence time. For each packet, we extract CSI for 56 subcarriers, which are equally distributed in a 20MHz channel.

We experiment with two types of commonly consumed fruits: kiwi fruit and avocado. The specific cultivars of avocado and kiwi fruit are Hass and Fuzzy respectively. Each type of fruit samples are purchased from two different vendors. Particularly, the production locations for kiwi fruits are USA and New Zealand for vender 1 and vender 2 respectively, whereas for avocado they are Mexico and USA for vender 1 and vender 2, respectively. The purchased fruits have four ripeness levels as commonly adopted by fruit industry: *unripen, half ripen, ripen* and *over ripen* [24], [31]. We use a spectrometer to log the ground truth of the fruit ripeness. For each ripeness level and each type of fruit, we have around 75 fruits under testing. Figure 6 shows the detailed break down for each ripeness stage, vender, and type of fruit. To build the fruit ripeness profiles, we pre-select 10 fruits at each ripeness level with various fruit sizes and average the features extracted from these fruits. All fruits are tested under the room temperature($23°C$ to $26°C$).

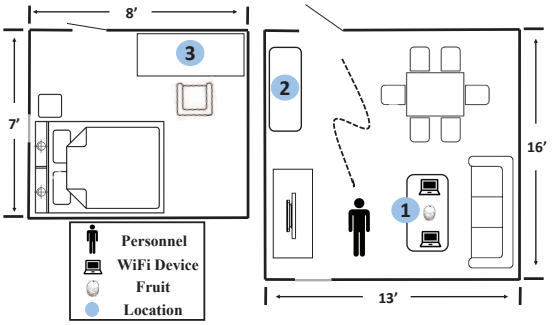

Fig. 7. Illustration of experiment setup.

(a) Kiwi (b) Avocado

Fig. 8. Confusion matrix of ripeness level detection for both kiwi and avocado fruits.

The experiments are conducted in two rooms at three locations, representing three different multipath environments. Figure 7 shows the layout of two rooms (i.e., one living room and one bedroom) and three locations. The bedroom has the size of 7 ft by 8 ft with one bed, one pair of table and chair. For the living room, it is 16 ft by 13 ft with regular living room furniture setup, such as dining table, book shelf, sofa, and TV. The bedroom environment represents a more compact space filled with furniture, while the living room setup describes a typical home environment with a larger space. To test the robustness of our system to the environment changes, we experiment with people walking around during the ripeness detection. In particular, during the data collection, a person is walking around in the room to create interferences. The walking trajectory is shown in dash curve in Figure 7.

We use confusion matrix and detection accuracy to evaluate our system performance. For confusion matrix, each column represents the fruit ripeness level that was classified by our system and each row shows the ground truth of the ripeness level. Each cell in the matrix corresponds to the fraction of ripeness level in the row that was classified as the ripeness level in the column. The detection accuracy is the percentage of the fruit that is correctly identified by our system.

B. Overall Performance

Figure 8 shows the confusion matrix of fruit ripeness detection for both kiwi and avocado. We observe that for both fruits, our system achieves overall detection accuracy over 90%. In particular, the overall detection accuracy for avocado

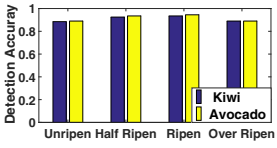

(a) Overall Accuracy

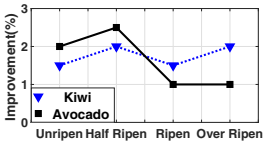

(b) Improvement

Fig. 9. Detection accuracy and improvement after separating the small and the large size fruits.

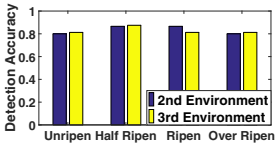

(a) Kiwi

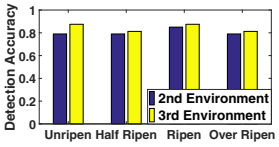

(b) Avocado

Fig. 10. Detection accuracy under two multipath environments when using the ripeness profiles built under a different multipath environment.

is about 91%, whereas it is 90% for kiwi. Moreover, the half ripen and ripen fruit detection, compared to unripen and over ripen fruit detection, has a higher detection accuracy for both kiwi and avocado. Specifically, ripen fruit detection achieves 93% and 94% accuracy for kiwi and avocado respectively. This is due to the fact that the physiological changes at unripen and over ripen levels are at slower pace, whereas the changes at half ripen and ripen levels go through faster processes [24]. Thus, more physiological changes of fruit at half ripen and ripen stages could be captured for ripeness detection. The above results show that our system could provide high accuracy in detecting fruit ripeness by using single pair of WiFi devices. The results also show that our system works with different multipath environments without location specific or environment specific calibration for ripeness profile. Still, the performance could be potentially improved by using additional pairs of WiFi devices or with multiple antennas.

C. Impact of Fruit Size

We next evaluate the performance when the testing fruits have similar sizes as that of the fruits used to build ripeness profiles. In particular, the size of kiwi varies from 55mm to 63mm, whereas it is from 69mm to 85mm for avocado. We classify each type of fruit into two categories: small fruits and large fruits. Then, we sense the ripeness of small (large) fruits with the profiles built from the small (large) size fruits. Figure 9 shows the the overall accuracy for separating small and large size fruits and corresponding improvement with respect to mixed size fruits. We find that our system achieves slightly better performance at each ripeness level detection for both kiwi and avocado. In particular, it achieves an overall accuracy at around 92% for both kiwi and avocado. The overall improvement is at around 2% when comparing to that of the mixed fruit case. The results show that our system is not very sensitive to the fruit size, although a more fine-grained fruit profile could slightly improve the accuracy.

D. Detailed Study on Multipath Environments

Although our overall performance in Section IV-B shows that our system works for different multipath environments,

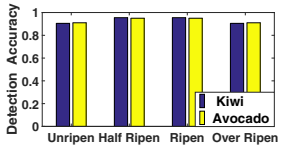

(a) Overall accuracy

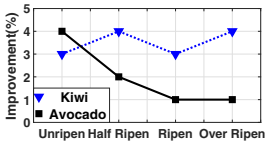

(b) Improvement

Fig. 11. Detection accuracy and improvement after separating fruit based on producing location.

we further perform a more detailed study on whether the performance changes when using the ripeness profile built at one multipath environment to test the fruits at a different multipath environment. Specifically, we build the ripeness profiles when the fruits are at the location 1 in Figure 7. We then use such profiles to detect the fruits that placed at the location 2 (in the same room), and location 3 (in a different room). Figure 10(a) and Figure 10(b) present the performance of ripeness detection for kiwi and avocado, respectively. We observe that our system does not suffer from performance degradation although the training and testing environments are under different multipath propagation. In particular, the overall detection accuracy still maintains at around 90% for both kiwi and avocado. These results further demonstrate the effectiveness of the multipath removal that leverages the larger bandwidth at 5GHz. It shows that our fruit ripeness detection system is location independent and environment independent. Once the profile is built, it can be applied to different environments without profile updating or calibration.

E. Impact of Fruit Producing Location

We next study the impact of production location of the fruit by separating each type of fruits based on their producing area. In particular, we build the ripeness profiles based on the producing area of each type of fruits. Then the ripeness profiles are used to test the fruits produced in the same area. The two producing areas for kiwi is USA and New Zealand, whereas they are USA and Mexico for avocado. The results are shown in Figure 11. We find that the detection accuracy has obvious improvement for both kiwi and avocado when compared to separating the fruits based on their sizes. Specifically, the overall accuracy is close to 94% for kiwi and at about 93% for avocado. The results show that the producing area of fruits plays an important role when building the profile, even for the same type of fruit. This is because different producing areas result in different percentage of dry matter and moisture content, which is also discovered by existing work [21]. It suggests that a more fine-grained profile based on producing areas could improve the ripeness detection accuracy.

V. Related Work

There have been wide ranges of work utilizing specialized or commodity RF devices to perform human sensing. For example, E-Eyes [30] is able to track daily activities and WiSee [25] uses specialized RF device to sense whole home gestures. Moreover, WiKey [5] has the ability to sense typing on keyboard, whereas system proposed by Liu *et al.* [19] is able to sense heartbeats and breathing. Besides motion and

activity tracking, many RF based localization systems have been proposed. For example, Chronos [28] achieves decimeter-level localization with a single WiFi AP, and WiTrack [4] utilizes RF body reflections to enable localization.

In general, the approaches for fruit ripeness detection can be divided into two categories: destructive and non-destructive methods. By measuring the sugar to acid ratio or total content of sugar or acid with refractometer, Jones and Scott [16] are able to track the ripeness level. Similar methods such as gas chromatograph [7] and mass spectrometer [26] can also be used to further analyze the chemical compounds of different fruits to identify different ripeness levels. Such methods however are destructive and compromise the intactness of sample and prevent it from future consumption.

For non-destructive methods, Peirs *et al.* [22] use NIR spectroscopy for post-harvest quality evaluation of apples. Imaging techniques such as X-ray computed tomography [14] and magnetic resonance imaging [6] have also been shown to be effective in fruit quality tracking. Moreover, ultrasonic signals have also been utilized to determine fruit maturity level [3]. The above approaches though provide non-destructive measuring, usually require expensive laboratory equipments. Recently, Das *et al.* [8] use portable spectrometer that senses the UV fluorescence of Chlorophyll for ripeness. Commercial devices such as SCiO [2] and Changhong H2 [1] can also achieve similar functionality using portable optical sensors. However, there are non-negligible costs incurred in purchasing dedicated spectral sensors.

VI. Conclusion

This paper presents FruitSense, which is capable of sensing the ripeness of fruit by analyzing wireless signals traveling through the fruit. The proposed system, FruitSense, is non-destructive and only requires a pair of off-the-shelf WiFi devices. The insight is that the signals traveling through the fruit could capture the physiological changes associated with fruit ripening. Experimental results under different multipath environments show that FruitSense can detect the ripeness levels of both kiwi fruit and avocado with an accuracy over 90%. FruitSense builds on the growing interest in using wireless signals for human sensing. The proposed work further expands the scope of human sensing to sensing the bio-information of fruit crops. We believe the implication of the work could be extended beyond classifying the fruit ripeness, particularly in quantifying the physiological compounds of fruit with more advanced signal process and machine learning techniques.

VII. Acknowledgements

This work was partially supported by the National Science Foundation Grands CNS-1514238, CNS-1816265, and CNS-1505175.

References

[1] Changhong. https://liliputing.com/2017/01/changhong-h2-smartphone-built-spectrometer.html, note = Accessed: 2017-03-29.

[2] Scio. https://www.consumerphysics.com/. Accessed: 2017-03-29.

[3] S. Adhimantoro and F. L. Gaol. Application of ultrasonic and fuzzy logic to determine fruit maturity level. *IJCAS*, 7(1):27–38, 2014.

[4] F. Adib, Z. Kabelac, and D. Katabi. Multi-person localization via rf body reflections. In *NSDI*, pages 279–292, 2015.

[5] K. Ali, A. X. Liu, W. Wang, and M. Shahzad. Keystroke recognition using wifi signals. In *ACM MobiCom*, 2015.

[6] P. Barreiro et al. Mealiness assessment in apples and peaches using mri techniques. *Magnetic Resonance Imaging*, 18(9):1175–1181, 2000.

[7] R. G. Buttery, R. Teranishi, R. A. Flath, and L. C. Ling. Fresh tomato volatiles. ACS Publications, 1989.

[8] A. J. Das, A. Wahi, I. Kothari, and R. Raskar. Ultra-portable, wireless smartphone spectrometer for rapid, non-destructive testing of fruit ripeness. *Scientific Reports*, 6, 2016.

[9] A. Goldsmith. *Wireless communications*. Cambridge university, 2005.

[10] D. Gunders. Wasted: How america is losing up to 40 percent of its food from farm to fork to landfill. *Natural Resources Defense Council*, pages 1–26, 2012.

[11] F. Harker et al. Penetrometer measurement of apple and kiwifruit firmness: operator and instrument differences. *JASHS*, 1996.

[12] R. Harrill. Using a refractometer to test the quality of fruits and vegetables. *P. PUBLISHING, Éd.) Consulté le July*, 20:2010, 1998.

[13] K. Hou et al. On the linear convergence of the proximal gradient method for trace norm regularization. In *NIPS*, pages 710–718, 2013.

[14] J.-A. Jiang et al. An adaptive image segmentation algorithm for x-ray quarantine inspection of selected fruits. *CEA*, 60(2):190–200, 2008.

[15] V. P. G. Jimenez, M.-G. Garcia, F. G. Serrano, and A. G. Armada. Design and implementation of synchronization and agc for ofdm-based wlan receivers. *IEEE Transactions on Consumer Electronics*, 2004.

[16] R. Jones and S. Scott. Improvement of tomato flavor by genetically increasing sugar and acid contents. *Euphytica*, 32(3):845–855, 1983.

[17] J. Juansah, I. Budiastra, K. Dahlan, and B. Seminar. Electrical behavior of garut citrus fruits during ripening changes in resistance and capacitance models of internal fruits. *IJET-IJENS*, 12(4):1–8, 2012.

[18] V. Komarov, S. Wang, and J. Tang. Permittivity and measurements. *Encyclopedia of RF and microwave engineering*, 2005.

[19] J. Liu, Y. Wang, Y. Chen, J. Yang, and X. Chen. Tracking vital signs during sleep leveraging off-the-shelf wifi. In *ACM MobiHoc*, 2015.

[20] L. S. Magwaza and S. Z. Tesfay. A review of destructive and non-destructive methods for determining avocado fruit maturity. *Food and bioprocess technology*, 8(10):1995–2011, 2015.

[21] F. Ozdemir and A. Topuz. Changes in dry matter, oil content and fatty acids composition of avocado during harvesting time and post-harvesting ripening period. *Food Chemistry*, 86(1):79–83, 2004.

[22] A. Peirs et al. Phpostharvest technology: Comparison of fourier transform and dispersive near-infrared reflectance spectroscopy for apple quality measurements. *Biosystems Engineering*, 81(3):305–311, 2002.

[23] D. B. Percival and A. T. Walden. *Wavelet methods for time series analysis*, volume 4. Cambridge university press, 2006.

[24] V. Prasanna, T. Prabha, and R. Tharanathan. Fruit ripening phenomena–an overview. *Critical reviews in food science and nutrition*, 2007.

[25] Q. Pu, S. Gupta, S. Gollakota, and S. Patel. Whole-home gesture recognition using wireless signals. In *ACM MobiCom*, 2013.

[26] P. Schreier, F. Drawert, and A. Junker. Identification of volatile constituents from grapes. *JAFC*, 24(2):331–336, 1976.

[27] S. Tan and J. Yang. Wifinger: leveraging commodity wifi for fine-grained finger gesture recognition. In *ACM MobiHoc*, 2016.

[28] D. Vasisht, S. Kumar, and D. Katabi. Decimeter-level localization with a single wifi access point. In *USENIX NSDI*, 2016.

[29] C. Wang, X. Zheng, Y. J. Chen, and J. Yang. Locating rogue access point using fine-grained channel information. *IEEE Transactions on Mobile Computing*, 16(9):2560–2573, 2017.

[30] Y. Wang et al. E-eyes: device-free location-oriented activity identification using fine-grained wifi signatures. In *ACM MobiCom*, 2014.

[31] R. Wills and J. Golding. *Postharvest: an introduction to the physiology and handling of fruit and vegetables*. UNSW press, 2016.

[32] Y. Xie, Z. Li, and M. Li. Precise power delay profiling with commodity wifi. In *ACM MobiCom*, 2015.